In Situ Acoustic Temperature Measurement During Variable-Frequency Microwave Curing

Cleon E. Davis, *Member, IEEE*, Anthony J. Dickherber, *Student Member, IEEE*, William D. Hunt, *Senior Member, IEEE*, and Gary S. May, *Fellow, IEEE*

***Abstract*—Variable-frequency microwave (VFM) curing can perform the same processing steps as conventional thermal processing in minutes, without compromising intrinsic material properties. With increasing demand for novel dielectrics, there is a corresponding demand for new processing techniques that lead to comparable or better properties than conventional methods. VFM processing can be a viable alternative to conventional thermal techniques. However, current limitations include a lack of reliable temperature measuring techniques. This research focuses on developing a reliable temperature measuring system using acoustic techniques to monitor low-k polymer dielectrics cured on silicon wafers in a VFM furnace. The acoustic sensor exhibits the capability to measure temperatures from 20 °C to 300 °C with an attainable accuracy of ±2 degrees.**

***Index Terms*—Acoustic temperature sensing, polymer curing, rapid curing, variable frequency microwave curing, zinc oxide deposition.**

I. Introduction

THE development of advanced materials plays a vital role in the manufacture of thinner, smaller, and faster electronic devices. The limitations of traditional inorganic dielectrics have driven the microelectronics industry to develop new organic, inorganic, and porous dielectric materials that have superior performance. As such, a number of research studies have been conducted to develop low-k and ultra low-k dielectrics for use in the semiconductor manufacturing industry [1], [2]. A considerable number of these novel dielectrics are polymers, polyimides, spin-on glasses, and porous materials. With increasing demand for novel dielectrics, there is a corresponding demand for new processing techniques that lead to comparable or better properties than conventional methods.

Currently, conventional thermal curing steps can take several hours, and there is a need to shorten the processing time for cost reasons [3]. A new thermal processing technique known as variable frequency microwave (VFM) curing can perform the same processing steps in minutes, without compromising the intrinsic material properties [4]–[6]. In the future, VFM processing could be a viable alternative to conventional thermal processing techniques because of advantages like rapid heating, selective heating of materials though differential absorption, penetrating radiation, controllable electric field distribution, and self-limiting reactions. However, current limitations in VFM processing include uncertain process characterization methods, lack of reliable temperature measuring techniques, and the lack of control over the various processes occurring in the VFM chamber. To address these issues, prior work has utilized experiment design, neural networks, and genetic algorithms to model and optimize the polymers cured on silicon using a VFM furnace [7], [8]. The current research addresses the challenge of a reliable temperature measuring device by the development of an acoustic temperature sensor for VFM processing monitoring.

The acoustic temperature sensor developed herein relies on the monotonic relationship between temperature and time-of-flight of longitudinal acoustic waves to monitor the temperature of silicon in the VFM furnace. In Section II, we discuss conventional and VFM curing of polymer dielectrics. In the VFM curing subsection, we discuss VFM processing in more detail. In Section III, a discussion on the background of acoustic temperature sensing is presented, and in Section IV, we present the acoustic temperature sensor design for this research. Results and discussion are presented in Section V. A conclusion is given in Section VI, and future work is discussed briefly in Section VII.

II. Polymer Curing

A. Conventional Curing

The objective of curing polymers in microelectronics is to remove residual solvents and to complete the chemical reactions that convert monomers into polymers. Because curing conditions play a major role in the final properties of a polymer, it is important to reduce variability when curing polymers so that acceptable electrical and mechanical properties result. Some of the parameters that must be controlled to ensure a proper cure include the polymer composition and molecular weight: glass transition temperature; time, temperature, and heating rate; and environmental conditions such as the atmosphere, relative humidity, exhaust flow rate [9]. For a given polymer with constant molecular weight and composition, the primary factors that control the curing process are time, temperature, and heating rate [9].

In microelectronic applications, minimizing stress is a very important issue. A ramped cure cycle is typically used to facilitate solvent removal and to minimize the development of

Manuscript received April 25, 2007; revised May 14, 2008. This work was supported by the Office of Naval Research and the National Science Foundation. This work was recommended for publication by Associate Editor J. Liu upon evaluation of the reviewers comments.

C. E. Davis is with the Johns Hopkins University Applied Physics Laboratory, Laurel, MD 20723 USA.

A. J. Dickherber, W. D. Hunt, and G. S. May are with the School of Electrical and Computer Engineering, Georgia Institute of Technology, Atlanta, GA 30332 USA.

Color versions of one or more of the figures in this paper are available online at http://ieeexplore.ieee.org.

Digital Object Identifier 10.1109/TEPM.2008.2004570

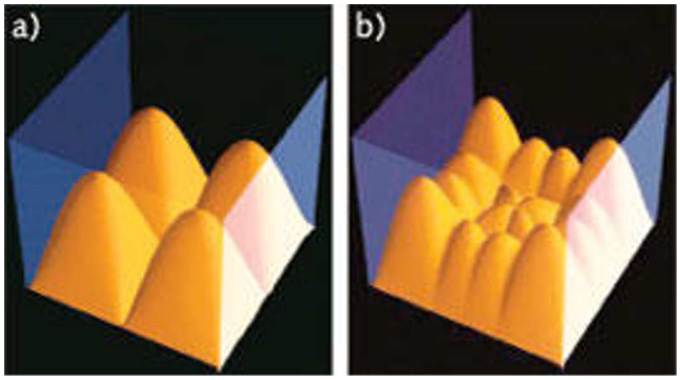

Fig. 1. Schematic representations of microwave energy distribution in cavities for (a) fixed frequency microwave and (b) variable frequency microwave [10].

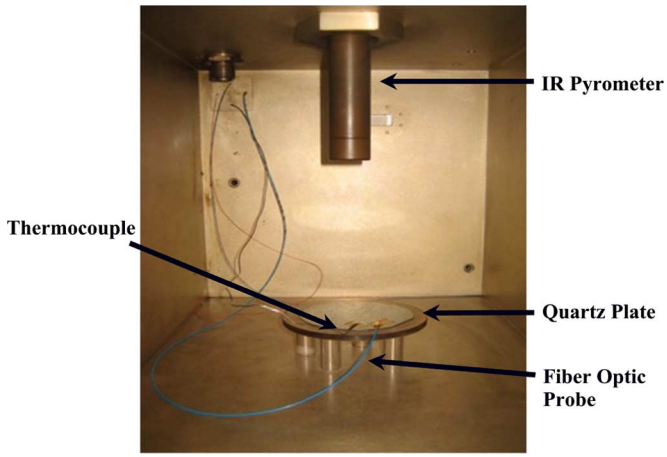

Fig. 2. Current temperature measuring devices.

thermal stresses arising from the coefficient of thermal expansion (CTE) mismatch between the polymer and the substrate [9]. To further reduce the potential for stress, polymers should not be cured above their glass transition temperatures. However, if a polymer is not fully cured, any subsequent processing of the film that exceeds the final cure temperature may result in the release of volatiles. Consequently, the final cure temperature should be at least as high as the maximum temperature of any subsequent processing [9].

A standard curing process is typically done in either a laminar flow forced air convection oven or in a diffusion furnace [9]. The primary requirements of the curing equipment are uniform temperature distribution, the capability to adequately control the heating rate, the capability to maintain a dry inert atmosphere (exclude moisture and oxygen), and the provision of adequate ventilation to remove volatiles that are released during the cure [9].

B. VFM Curing

In this paper, VFM curing is performed in a MircoCure 2100, which is manufactured by Lambda Technologies in Research Triangle Park, NC. The controllable parameters for the MicroCure 2100 are center frequency, bandwidth, sweep rate, power level, and ramp rate. Samples may be processed at a fixed frequency, at a variable frequency with a specific center frequency and bandwidth, with a varying bandwidth, and/or varying sweep rate. However, the unique feature of this system is the capability of frequency stepping. The system can step through 4096 frequencies over a 1.15-GHz bandwidth every 0.1 s. This frequency stepping provides a time-averaged uniform energy distribution throughout the cavity, which eliminates the nonuniform temperature distribution that occurs in single-frequency microwave furnaces as shown in Fig. 1.

This VFM furnace also has a feedback control system that regulates the temperature of the sample being processed. The control system can automatically adjust the power levels to maintain the sample at the desired temperature, which allows good control of ramp rates and final hold temperatures of the samples to be processed. The VFM furnace has provisions to maintain an inert atmosphere during processing of samples. The processing cavity can be pumped down using a mechanical pump and back-filled using nitrogen gas for processing in an oxygen-free environment. Another important characteristic of a VFM furnace is the ability to place metal inside the microwave cavity because charge build up and arcing due to the presence of the field is eliminated.

Three temperature measurement devices are currently used in the VFM furnace: an infrared pyrometer, a fiber optic probe, and a thermocouple. The pyrometer is a noncontact device, whereas the thermocouple and fiber optic probe need to be held in contact with the substrate with high-temperature Kapton tape and a metal clip insulated with the tape a metal clip insulated with the tape, as shown in Fig. 2. Despite the availability of several temperature measurement techniques for the VFM, a consistent measurement technique is still needed to accurately process materials. This is attributed to the physical contact needed to be established to use the fiber optic probe and thermocouple, and the varying emissivity values for the range of temperatures required to set the pyrometer temperature level. The emissivity depends on factors such as temperature, surface roughness, and wavelength. Since these parameters are changing during a cure, there is no automated way to determine the emissivity of a sample. Even if there was an automated method to determine the emissivity, the current pyrometer has the limitation of a manual input for the emissivity value.

When processing in the VFM furnace, a sample is placed on a quartz substrate, which is supported by quartz mounts. The fiber optic probe and thermocouple are attached to the sample. The experimental data is usually taken with the infrared pyrometer as the temperature measuring and control device, with the fiber optic probe acting as the temperature verification sensor. A calibration step must be performed to determine the emissivity of a sample. The emissivity of the pyrometer is then set to the final cure emissivity of the polymer.

Curing polyimide involves the removal of solvent or other volatiles from the film and the imidization (or hardening) of the polymer into an intractable polyimide film.[1] The curing process is performed in several steps. Hot plates are commonly used for a soft bake after the polymer is applied. Post bakes range from 50 °C–150 °C on one or more inline hot plates. Typically, a furnace or programmable oven is then used for the final cure. Final

[1][Online]. Available: http://www.hdmicrosystems.com/tech/process.html.

curing is usually done at temperatures between 280 °C–400 °C, depending on the application.

For a typical experiment, PI 2611 was spun-cast onto silicon wafers and subsequently soft baked at 120 °C for 2 min on a hotplate. The spun-on film thicknesses were in the range of 18 –22 μm. The coated wafers were then cured in the VFM furnace under a nitrogen atmosphere. During VFM processing, the temperature of the polyimide samples were ramped to an appropriate level and held there for a specific amount of time. After curing, the wafers are allowed to cool to room temperature. After cooling, measurements are taken to determine electrical and mechanical properties of the films. The cured film thicknesses were in the range of 10–12 μm. To improve process monitoring for the VFM system (with the goal of better control of the heating rate and temperature), an acoustic temperature sensor was developed and implemented in the VFM furnace to monitor polymer dielectric curing on a silicon wafer.

III. Acoustic Temperature Sensing

One limitation of VFM processing is the lack of reliable temperature measuring devices. This limitation reduces the capacity to effectively monitor and control temperature while processing in a VFM furnace. A novel approach to temperature measurement is acoustic temperature sensing. An acoustic temperature sensor (ATS) is typically developed based on one of two phenomena: 1) the change in acoustic velocity as a function of temperature [11], and/or (2) the phase-shift of acoustic wave as it is reflected from an interface as a function of temperature [12].

For many years, researchers have exploited the concept of measuring the temperature of a gas by measuring the speed of sound in that gas. This is a technique known as acoustic pyrometry [13], [14]. Sensors based on this phenomenon have been developed for real-time temperature profile measurements inside automobile catalytic converters and industrial furnaces and boilers. Another example of change in acoustic velocity being used to measure the temperature is that of the slotted acoustic rod [15], where ultrasonic pulses are excited in an acoustic rod with known expansion and propagation properties. For a rod with notches at known distances from the excitation position, the temperature of the medium can be calculated by measuring the reflection times of the pulses from the notches.

In the 1990s, several acoustic sensors were developed at Stanford University [11], [19]. One of these was used to measure the temperature in a wafer by exploiting the interdependence of the Lamb wave acoustic velocity and temperature of silicon [11], [16]. This device was used to measure the temperature in a rapid thermal processing system. In addition to measuring temperature, this technique was used to determine the film thickness on the same substrate that temperature was being measured by using two sets of transducers operating at different frequencies [18]. In [19], Lee and others developed a noninvasive technique to measure temperature using a laser to excite acoustic waves in a substrate and then exploited the change in the dispersion relations of the plate modes through the wafer as a function of temperature. In the late 1990s, the Stanford group developed an ultrasonic sensor that was used to monitor pre-bake photoresist processing [12], [20].

Temperature sensors have also been developed based on other acoustic wave phenomena. Surface acoustic waves (SAWs) and surface skimming bulk waves (SSBWs) have also been used to measure temperature of films [21], [22].

The acoustic temperature sensor developed in the present study measures the temperature of a polymer-coated silicon wafer in a variable frequency microwave furnace. The time-of-flight of an acoustic wave in silicon is related to the temperature through the dependence of the elastic constants [16], [17], [23]. In the seminal paper by McSkimm [23], acoustic velocity was characterized as a function of temperature in silicon. This data showed that the acoustic velocity decreases as temperature increases, which corresponds to a negative velocity coefficient of temperature (-31e-6 [dimensionless quantity]). Thus, there is an increase in the time-of-flight of the acoustic wave when the silicon temperature increases.

IV. Sensor Design

A. Piezoelectricity

A piezoelectric transducer converts electrical signals into mechanical signals and vice versa [24]. One of the more widely used piezoelectric materials for acoustic applications is zinc oxide (ZnO). Zinc oxide has been widely used because of its relatively high coupling coefficient (0.28 [25]), the fact that it adheres well to a number of substances, and because its methods of deposition coincides with IC fabrication techniques [26]. Zinc oxide has been used for acoustic devices such as SAW devices [27], [28], surface skimming bulk wave [21], flexural plate wave devices [29], lamb wave devices [16], [17], bulk acoustic wave devices [27], [30], longitudinal wave devices [12], and acoustic–optic devices.

1) Zinc Oxide Deposition: The deposition of ZnO is very important because the thickness of a transducer determines the fundamental operating frequency for the device [31] and because the film quality (crystalline structure, lack of voids, etc.) determines if a device will be peizoelectrically active or not. Lee *et al.* reported that polycrystalline ZnO thin films must meet two requirements to be properly suited for acoustic wave devices: 1) the basal plane of ZnO crystallites must be oriented parallel to the plane of the substrate, which is sometimes referred to as "c-axis orientation"; and 2) the ZnO film must have a columnar structure with void-free boundaries [32].

Zinc oxide can be deposited in a number of ways: RF magnetron sputtering [27], [28], [32], dc magnetron sputtering [35], [36], dc triode sputtering [27], [28], molecular beam epitaxy [37], metal organic chemical vapor deposition (MOCVD) [38], and pulsed laser [39]. ZnO can be deposited by sputtering a zinc target in an oxygen atmosphere [33], [35] or sputtering a ceramic ZnO target [25]. RF sputtering of a ceramic ZnO target is the most common method of deposition. Because of the number of techniques and system configurations for a particular method, there has been a considerable amount of research conducted on processing, characterizing, and optimizing (trying to produce highly c-axis oriented) ZnO films [25], [26], [30], [32], [34], [40].

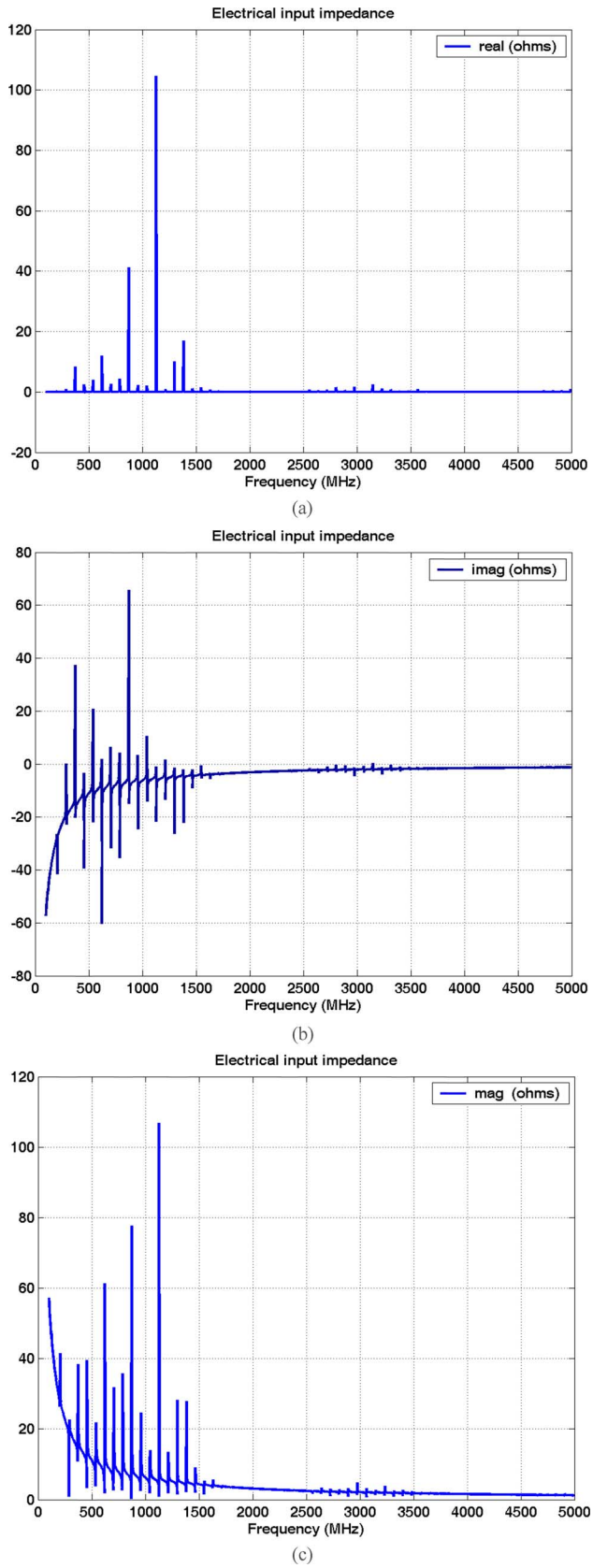

Fig. 3. Input impedance (a) real, (b) imaginary, and (c) magnitude from KLM model showing that the sensor should resonate around 200 MHz to 1.6 GHz.

Although the techniques used to deposit ZnO come from the IC domain, ZnO is highly reactive. After it is deposited, subsequent processing can contaminate processing chambers as well as other device fabricated on silicon [26]. However, a passivation layer of silicon nitride can help reduce device contamination [41].

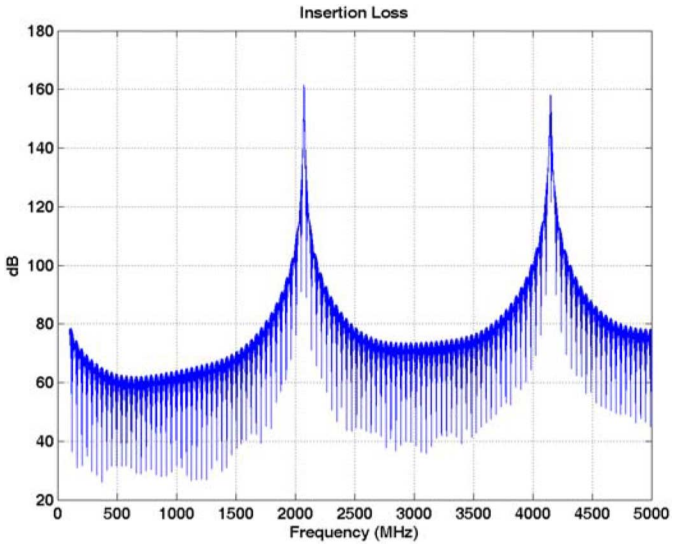

Fig. 4. Insertion loss of transducer from KLM model.

2) Sensor Modeling: To facilitate the design of acoustic devices and to gain a better understanding of the affects of changing a transducer's parameters, a model was developed of the acoustic device. There are two major approaches for modeling acoustic devices: Mason's lumped-element circuit model [24], [42], [43] and the Krimholt–Leedom–Matthaei (KLM) model [44]. These modeling techniques can be use to determine the resonant frequency and insertion loss of devices. They may also be used to optimize transducer parameters such as film thickness, transducer area, type of transducer material, type of contact, and contact thicknesses. Mason's model is a one-dimensional, lumped-element equivalent circuit model of a piezoelectric device. It consists of an equivalent circuit that separates the piezoelectric material into an electrical port and two acoustic ports through the use of an ideal electromechanical transformer, where network theory can be used to analyze the circuit [45]. One of the drawbacks of the Mason's model is that it contains a (nonrealizable) negative capacitance [42]. The KLM model is also a three-port network, but the equivalent circuit models an acoustic device using transmission line theory.

For this research, a KLM modeling program that was developed in the Ginzton Laboratory by Gokhan Percin (circa 1997 [46]) was used. Fig. 3 illustrates the input impedance of the acoustic device parameters listed in Table I. This figure shows that the device should have a bandwidth of 200 MHz to 1.6 GHz with a center frequency of 700 MHz. The insertion loss, the loss resulting from a device being inserted into a transmission line, is plotted in Fig. 4. Low insertion loss is a design goal.

B. Sensor Fabrication

To fabricate the acoustic temperature sensor, a ZnO piezoelectric transducer was deposited onto a sapphire acoustic buffer rod. Sapphire was used as the acoustic buffer rod because it is inert to microwave radiation [4] and has a low acoustic attenuation [42]. First, the sapphire buffer rod was

TABLE I
ACOUSTIC DEVICE PARAMETERS USED IN THE KLM MODELING

Acoustic Device Parameters	
Buffer rod length	4.7 mm
Active transducer area	1 mm^2
ZnO Thickness	3 μm
Contact Thicknesses (Au)	1500 Å

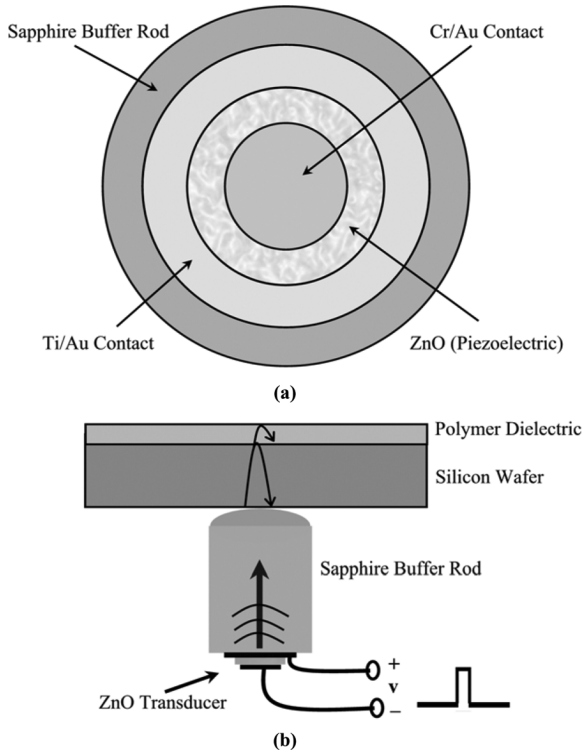

Fig. 5. (a) Illustration of a zinc oxide transducer fabricated on a sapphire buffer rod and (b) an ultrasonic wave traveling through acoustic temperature sensor.

ultrasonically cleaned with acetone, methanol, and isopropanol. Then, the piezoelectric transducer was fabricated by depositing a bottom contact of Ti/Au, a ZnO layer, and a top contact of Cr/Au onto the flat polished surface of the sapphire buffer rod. The bottom contact was deposited by electron-beam evaporation with the titanium layer, approximately 100 Å thick, serving as an adhesion layer. The gold layer was 1500 Å thick. The ZnO layer was deposited by RF sputtering at a temperature of 325 °C. The top contact consisted of 100 Å of chromium, which serves as an adhesion layer, and 1500 Å of gold, both deposited by electron-beam evaporation. Fig. 5 illustrates a fabricated transducer on a sapphire buffer rod.

Applying a voltage pulse between the two metal layers of the transducer generates a longitudinal wave in the transducer that is transmitted to the buffer rod. The longitudinal wave travels through the buffer rod, the wafer, and the polymer. The wave reflected from the wafer/air interface and/or polymer air interface back to the transducer. Temperature is subsequently calculated from the time-of-flight measurement. Fig. 5(b) shows a wave traveling through a buffer rod and wafer being reflected at the polymer–air interface.

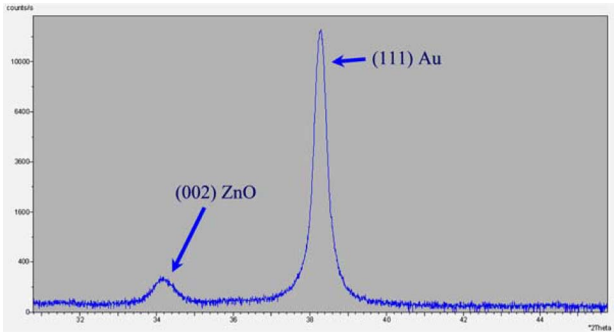

Fig. 6. XRD plot illustrating the (002) orientation of a ZnO film deposited on Au/Ti/ sapphire wafer.

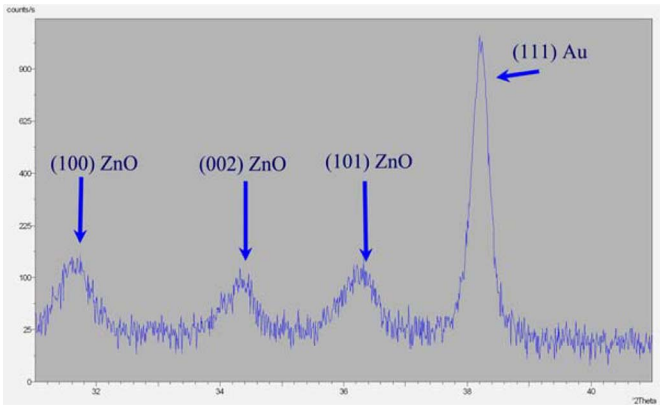

Fig. 7. XRD plot illustrating a polycrystalline ZnO film with (001), (002), and (101) orientations deposited on Au/TI/sapphire wafer.

C. Sensor Measurements

1) X-Ray Diffraction: In order for the transducer to resonate properly, the zinc oxide must have the correct crystal orientation (c-axis orientation). To determine the crystalline structure of the ZnO, X-ray diffraction (XRD) measurements were performed using a Phillips X'PERT Pro X-ray Diffractometer using Cu–Kα radiation. XRD ($\Omega-2\theta$ scan) measurements were taken of ZnO films that were deposited on the titanium/gold bottom contact, which had been deposited on 430-μm, double-sided double-polished, 2-in, c-axis oriented, sapphire wafers. It should be noted, that these films were deposited using the same recipe that was used for the buffer rod (see Table II). The thicknesses of the films were approximately 3 μm. The XRD measurement shown in Fig. 6 was taken from a film deposited by the Acoustic Electronics Group (AEG) at the Georgia Institute of Technology using an RF sputterer, while the XRD plot shown in Fig. 7 was of a film that was not deposited by the AEG. Table I lists typical RF sputterer parameters [30]. Fig. 6 illustrates a ZnO with the proper (002) orientation, which has a peak around 34.1 (2θ degrees). The XRD plot in Fig. 7 illustrated a polycrystalline ZnO film with the (001), (002), and (101) orientations. The films with this type of XRD scan can be thought of a poor quality, and these types of films were not piezoelectrically active when a top electrode was deposited and a voltage was subsequently applied to the contacts. Thus, these films did not produce transduction and were not used for the acoustic temperature sensor.

TABLE II
TYPICAL SPUTTERING PARAMETERS DEPOSITED BY THE MICROELECTRONIC ACOUSTIC GROUP AT THE GEORGIA INSTITUTE OF TECHNOLOGY [30]

Sputtering parameters	
RF Power	125 W
Argon Partial Pressure	2 mTorr
% Oxygen	3%
Deposition Pressure	5 mTorr
Temperature	325°C

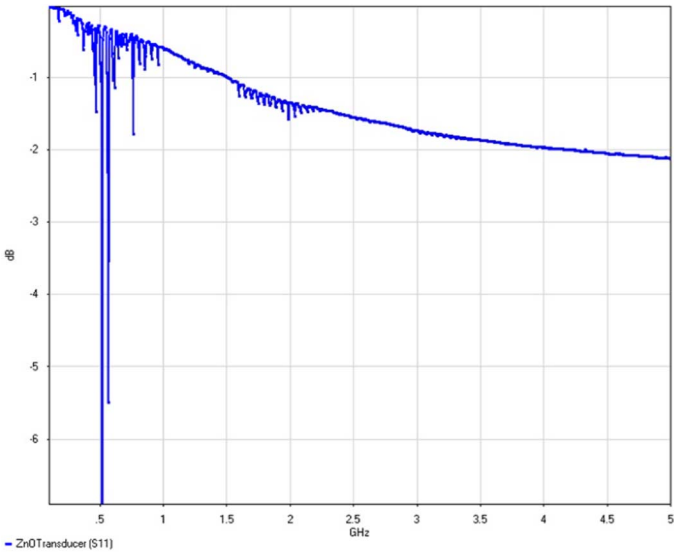

Fig. 8. ATS s-parameter measurement from 100 MHz to 5 GHz.

2) Network Analyzer Measurements: To determine if the transducer is active and to validate the operating frequency range of the sensor, scattering parameter (s-parameter) measurements were taken with an Agilent 85107B vector network analyzer (VNA). In general, s-parameters relate incident and reflected traveling waves that are scattered when an n-port network is inserted into a transmission line, and they provide a means of measuring and characterizing circuit elements when traditional lumped equivalent circuit models cannot accurately predict circuit behavior [47]. Thus, they can be used to determine properties of a circuit or network, such as gain, loss, reflection coefficient, etc.

In this paper, the reflection parameter s_{11}, which is the ratio of the reflected signal to the incident signal over a given frequency range, was measured. The s_{11} measurement is commonly transformed to yield the input impedance response Z_{in} of the network through the relationship

$$Z_{\text{in}} = 50 \cdot \frac{1 + s_{11}}{1 - s_{11}}. \tag{1}$$

To perform the VNA measurements, a calibration was performed using a standard short-open-load (SOL) technique. After calibration, the s_{11} data was collected. Fig. 8 is a plot of the s_{11} data for the ATS measured from 100 MHz to 5 GHz. From this measurement, it can be seen that the sensor has a bandwidth from 200 to 900 MHz with a center frequency of approximately 600 MHz. Fig. 9 consists of four plots: a) the real part of the input impedance measurements, b) imaginary part of the input impedance measurements, c) the magnitude of the

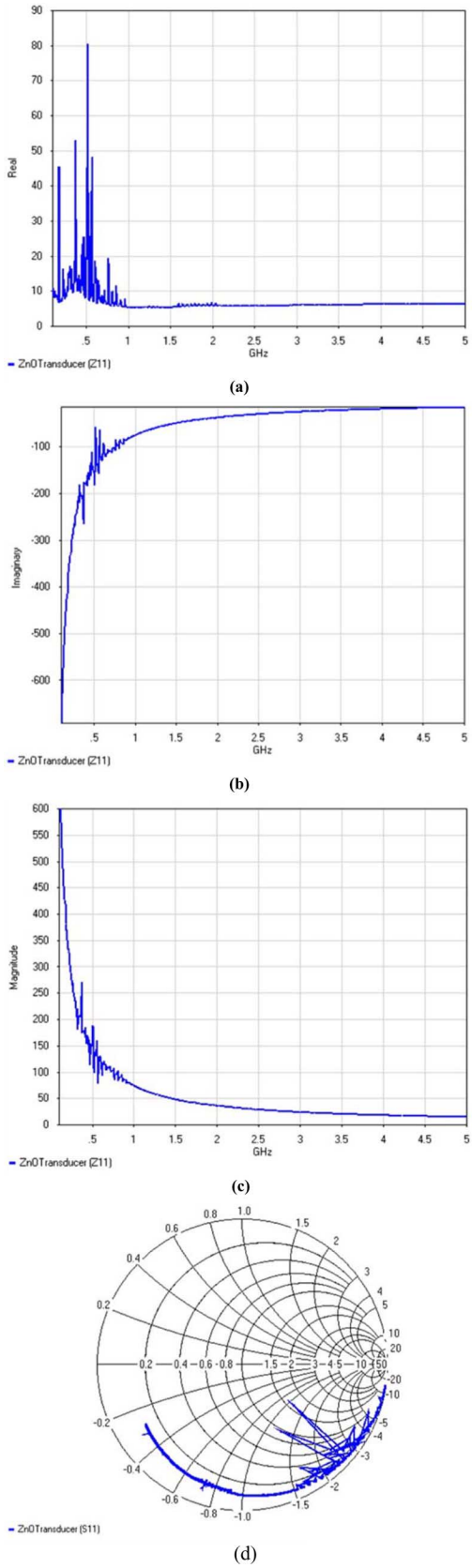

Fig. 9. (a) Real part of the input impedance measurements, (b) imaginary part of the input impedance measurements, (c) input impedance measurements, and (d) s-parameter measurements plotted on a Smith chart from 100 MHz to 5 GHz.

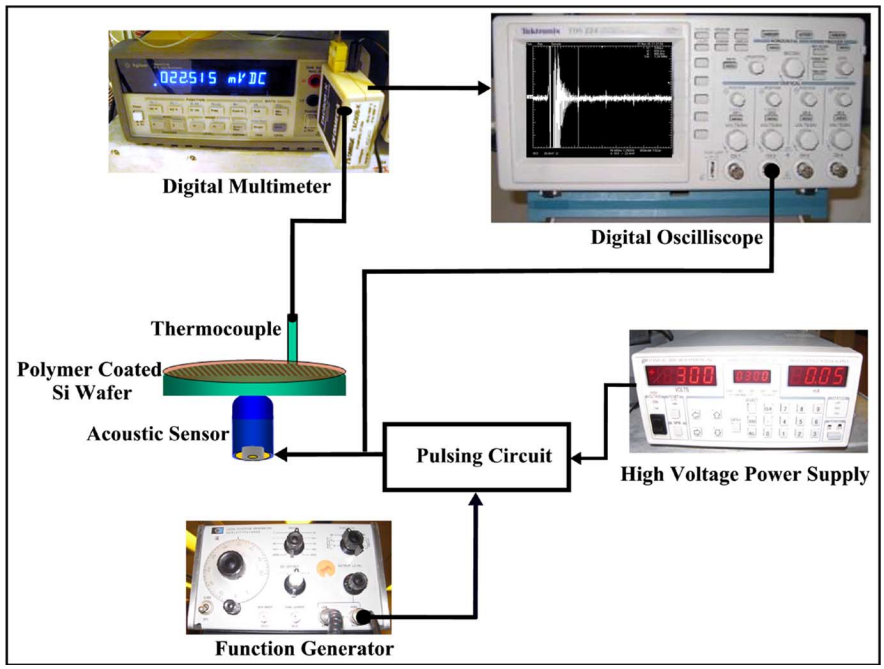

Fig. 10. Calibration schematic.

input impedance measurement, and d) s-parameter measurements plotted on a Smith chart from 100 MHz to 5 GHz.

V. Results and Discussion

A. Sensor Calibration

Before the acoustic temperature sensor was used in the VFM system, it was calibrated to determine the temperature sensitivity. Fig. 10 illustrates the ATS calibration process. First, the silicon wafer was heated on a hot plate. The ATS was placed in contact with the silicon wafer, and a high-voltage pulsing circuit is used to generate a 100-V, 90-ns pulse that produces a longitudinal wave in the sapphire rod. Time-of-flight measurements were made by monitoring the returned pulses of the sensor using a computer-controlled digital oscilloscope (Tektronix TDS 5054). A thermocouple was placed in contact with the wafer, and its readings were monitored with an Omega TAC80B-K thermocouple-to-analog converter connected to an Aglient 34401A digital multimeter, which was linked to the oscilloscope via an RS 232 serial connection.

The expected time-of-flight is calculated by dividing the buffer rod length (4.7 mm) by the speed of sound in sapphire (11 000 m/s) and multiplying that by a factor of two (for the two-way travel). This time was 854.5 ns. Fig. 11 is a typical oscilloscope reading with the initial pulse, followed by several returned pulses. The returned pulses are approximately 805 ns apart. Fig. 12 is an oscilloscope image of one of the returned pulses.

A MATLAB script was developed to locate the returned pulses and measure the time-of-flight as the temperature changed. The program captures a digitized averaged waveform from the oscilloscope. Returned pulses were identified by applying a moving window across the samples of the waveform and evaluating each sample in the window to a threshold.

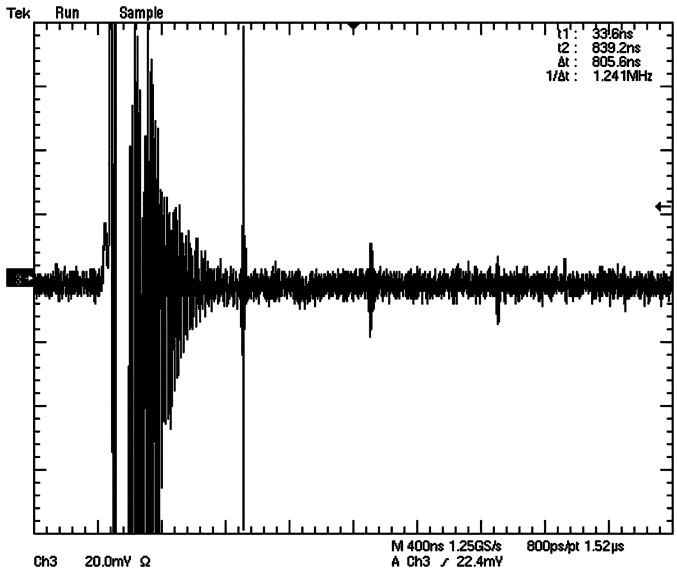

Fig. 11. Oscilloscope measurement showing initial pulse and several returned pulses.

The first waveform sample value in a particular window that was greater (or less) than the maxima (or min) threshold was classified as a returned pulse. After the first two pulses were found, the time-of-flight calculation was made by dividing the number of samples between the first and second pulses by the sampling rate. The top plot in Fig. 13 illustrates three returned pulses, where the program has identified the first two pulses and has placed a small circle at the leading edge of the pulse and plotted the pulses a different color than the waveform. Fig. 14(a) illustrates an approximately linear relationship of the time-of-flight of the returned pulses and the temperature. A polynomial model was developed from the data in Fig. 14(a)

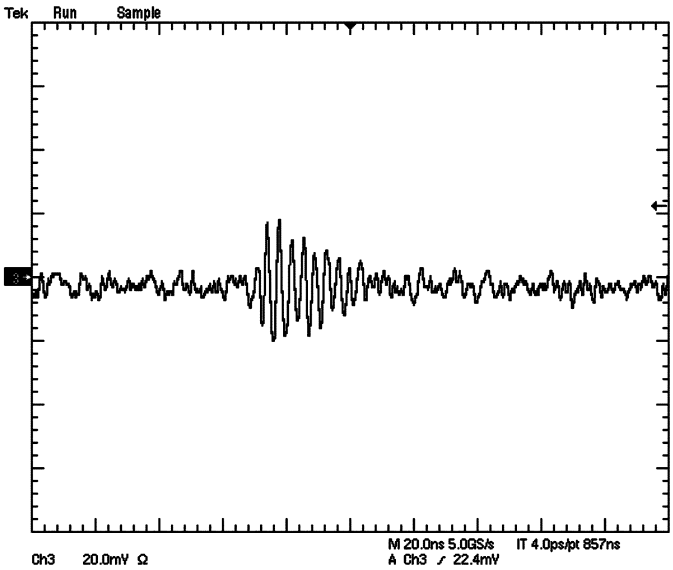

Fig. 12. Oscilloscope measurement showing one of the returned pulses.

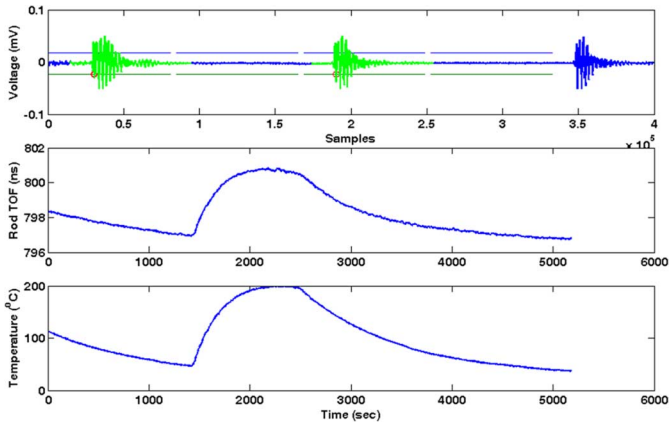

Fig. 13. ATS with temperature ramped to 200 °C and held there for approximately 5 min.

and used to plot the measured temperature of a thermocouple with the temperature estimate using the acoustic temperature sensor [Fig. 14(b)]. The plot shows that there is an attainable ± 2 degree error during ramp up and hold, but there is a ± 5 degree error during cool downs.

Fig. 15 illustrates the ATS measuring temperature that is ramped at a rate of 10 °C/min to 300 °C and held for approximately 80 min. At several points during the measurement, there are spikes in the time-of-flight data, which correspond to the algorithm not being able to capture one of the leading edges of the subsequent returned pulses.

B. ATS Implementation in VFM

To implement the acoustic temperature sensor in the VFM oven, the sensor had to be placed in a holder. The sensor holder was developed such that it was the same size as the quartz rod and plate that were already being used in the VFM. The ATS was set in the holder such that the sensor protruded less than a half a millimeter out of the holder. In this way, when a wafer is placed on top of the holder, it stays in contact with the sensor.

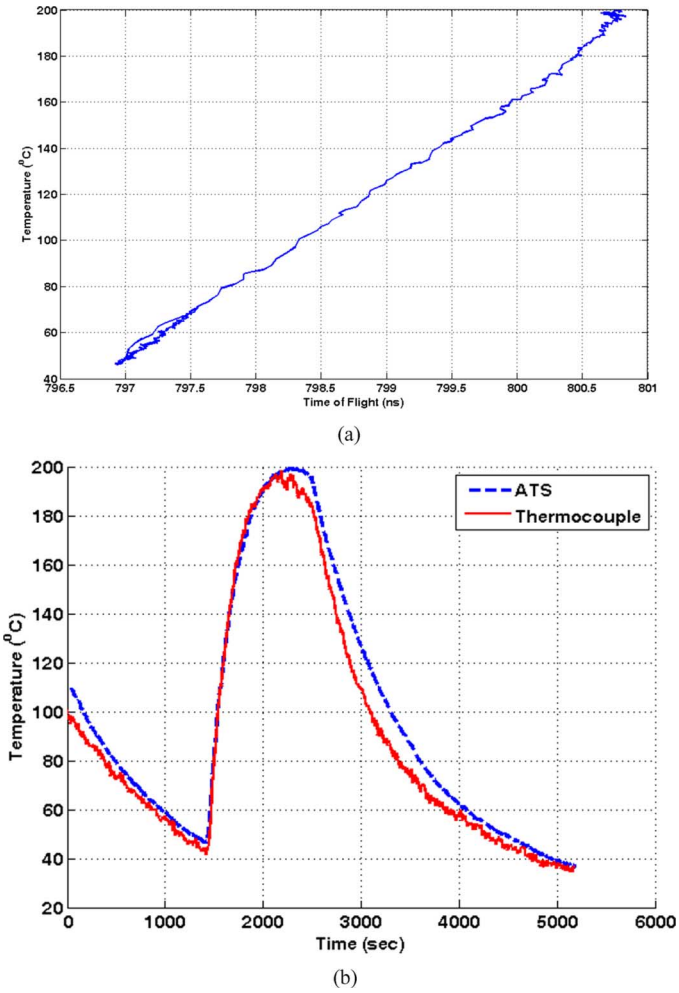

Fig. 14. (a) Effective temperature as a function time-of-flight and (b) plot of an acoustic temperature sensor measurement and the corresponding thermocouple measurement.

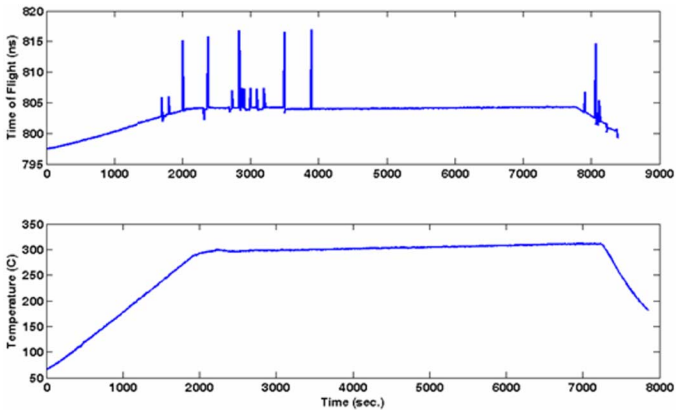

Fig. 15. ATS with temperature ramped to 300 °C and held there for approximately 80 min.

Wire bonding was attempted to attach the sensor fabricated on the buffer rod to the connector on the sensor holder. However, the bond between the gold wire and the top contact on the buffer rod was not strong enough (when a bond was actually made) and did not stay attached during subsequent processing. After examination of the surface of the top contact, it was found that

(a) (b)

Fig. 16. (a) ATS in the sensor holder next to the quartz plate and (b) shows a polymer-coated silicon wafer on top of the ATS in the sensor holder.

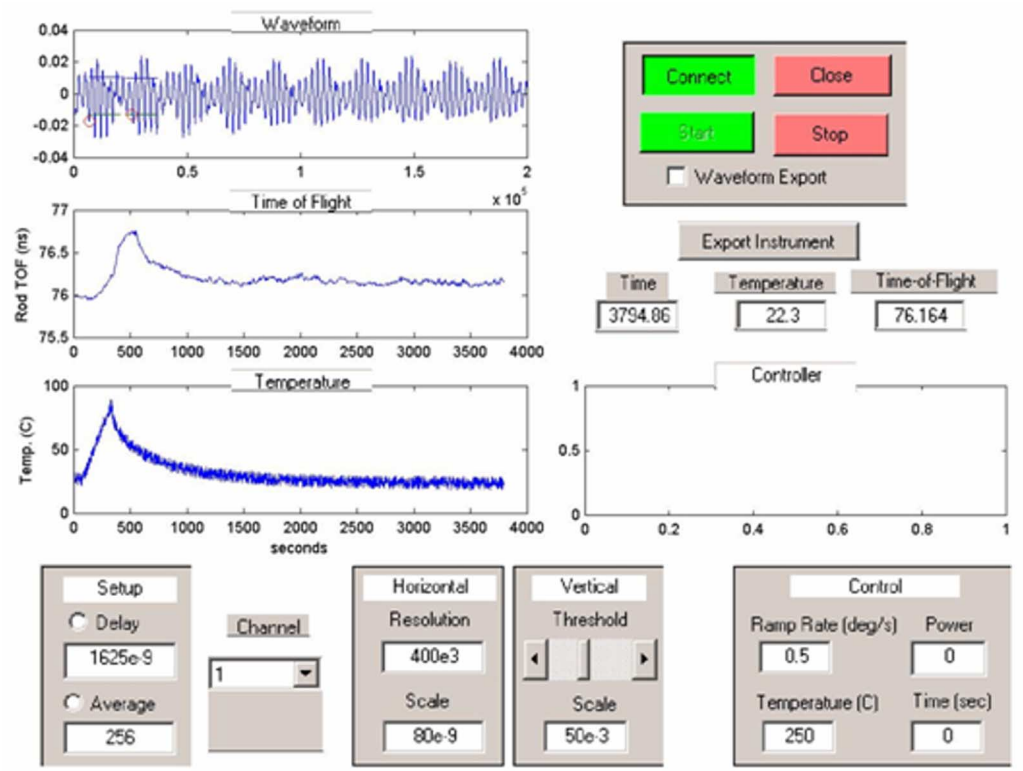

Fig. 17. Graphical user interface used to monitor *in situ* the returned pulses and the thermocouple readings of a polymer-coated wafer inside the VFM chamber.

the surface was very rough. In addition, the clamps on the wire bonder were not designed for circular devices, which meant that the buffer rod was not properly clamped down during bonding that could have caused the device to move during the ultrasonic phase of the bonding process. Because of this bonding issue with the transducer fabricated on to the buffer rod, the actual acoustic device that was implemented in the VFM furnace was fabricated on the double-sided polished sapphire wafer that was used for the XRD measurements with a top contact deposited on it. This acoustic sensor was mounted on to a sensor holder as described above. The sensor holder was placed inside the microwave chamber, and a polymer coated wafer was placed on top of the sensor/sensor holder (see Fig. 16).

A graphical user interface (GUI) was developed in MATLAB to monitor the time-of-flight from the returned pulses and to monitor the thermocouple that was attached to a polymer-coated wafer inside the VFM furnace. Fig. 17 illustrates the GUI with the temperature being ramped from room temperature to 95 °C. This figure shows that the profile of the returned pulses has a strong correspondence to the temperature profile from the thermocouple that was attached to the polymer coated wafer. The time-of-flight measurement is noisier in the VFM than it was

during calibration, which may be the result of the alternating field around the wires inside the VFM chamber that connect the ATS to the pulsing circuit. Both thermocouple and the ATS measurement would suffer from this problem. However, in a future version of the ATS, the wires could be shielded or the sensor could be designed so that the wires do not need to be inside the chamber.

VI. Conclusion

An acoustic temperature sensor was developed by depositing a ZnO transducer onto a sapphire buffer rod or sapphire wafer. Piezoelectric activity of the ZnO was confirmed by XRD measurements. The time-of-flight of a longitudinal wave acoustic wave was measured by generating a high voltage pulse, which produces the acoustic wave in the transducer. The acoustic wave travels through the sapphire into the silicon wafer and reflects off of either the silicon/air interface (or polymer/air interface if the silicon is coated with a polymer) and returns back to the transducer which then converts the mechanical signal back to an electrical signal, where it is read on an oscilloscope.

A MATLAB program was developed to capture the waveform from the oscilloscope and find the returned pulses within the waveform and by doing so measure, the time-of-flight as the temperature changed. The data exhibited an approximately linear relationship to the time-of-flight of the returned pulses and the temperature. The expected time-of-flight for the buffer rod was calculated by dividing the length of the rod (4.7 mm) by the speed of sound in sapphire (11 000 m/s) and multiplying that by a factor of two (for the two-way travel time), which was 854.5 ns. The actual returned pulses were approximately 805 ns apart. Experimental data was taken with the acoustic buffer rod measuring the time-of-flight of silicon wafers with temperature profiles ramped to as high as 300 °C and held constant for as long as 80 min. For lower temperature and shorter runs, the time-of-flight data was approximately linear with the temperature as measured with a thermocouple.

When the sensor was mounted in a holder and placed inside the VFM furnace, MATLAB with a GUI was used to monitor both the time-of-flight of the returned pulses and a thermocouple that was attached to a polymer-coated wafer. The time-of-flight data had a strong correspondence to the temperature profile from the thermocouple that was attached to the polymer-coated wafer. The acoustic sensor can measure temperatures from 20 °C to 300 °C with an attainable accuracy of ±2 °C.

VII. Future Work

To implement the scheme in a production VFM system, a redesign of the sensor holder may be required. Currently, the sensor holder is made of aluminum, but developing a sensor holder using a nonmetal such as quartz may be beneficial. The insulation of the wire that was used to contact the sensor in the VFM was burned during one of the runs. Thus, the insulation should be inert to microwave radiation. A potentially better approach would be to have the sensor mounted such that the wire contacts the transducer outside of the chamber, where no wires would be needed inside the chamber.

To further improve the monitoring capabilities of the VFM furnace, other sensors will be investigated. Some of the following sensors should be explored for *in situ* monitoring of VFM curing: Fourier transform infrared spectroscopy (FTIR), dual-wavelength IR pyrometer, and ellipsometer. In general, there is more information contained in the returned pulses from a transducer than the time-of-flight information. For example, the amplitude of the returned pulse can be used to determine the reflection coefficient. Further investigation will determine if this information, in addition to using a network analyzer to measure the phase of returned pulses, could be useful for VFM processing.

Acknowledgment

The authors would like to thank Prof. P. Kohl and Prof. F. L. Degertekin of the Georgia Institute of Technology for their assistance with VFM processing and the acoustic temperature sensor, respectively. The authors would also like to thank the technical staff at Lambda Technologies, Inc., for their assistance with maintenance of and technical advice with the VFM system.

References

[1] J.-W. Kang, B. R. Kim, G.-G. Kang, M.-S. Moon, B.-M. Choi, and M.-J. Ko, "New hybrid low-K dielectric materials prepared by vinylsilane polymerization," in *Proc. Mater. Res. Soc. Symp.*, 2004, pp. 25–30.

[2] J. J. Senkevich, C. Jezewski, D. Lu, W. A. Lanford, G.-C. Wang, and T.-M. Lu, "Molecular caulk: A pore sealing technology for ultra-low-K dielectrics," in *Proc. Mater. Res. Soc. Symp.*, Warrendale, PA, 2004, pp. 3–12.

[3] T. Wang and J. Liu, "A review of microwave curing of polymeric materials," *J. Electron. Manuf.*, vol. 10, pp. 181–189, 2000.

[4] R. V. Tanikella, "Variable frequency microwave processing of materials for microelectronic applications," Ph.D. dissertation, Chem. Eng., Georgia Inst. Technol., Atlanta, 2003.

[5] K. D. Farnsworth, R. Manepalli, S. Bidstrup-Allen, and P. Kohl, "Variable frequency microwave curing of 3, 3′, 4, 4-Biphenyltetracarboxylic acid dianhydride/P-phenylenediamine (Bpda/Ppd)," *Int. J. Microelectron. Packag.*, vol. 23, pp. 162–171, 2000.

[6] K. D. Farnsworth, R. N. Manepalli, S. A. Bidstrup-Allen, and P. Kohl, "Variable frequency microwave curing of photosensitive polyimides," *IEEE Trans. Compon. Packag. Technol.*, vol. 24, no. 3, pp. 474–480, Sep. 2001.

[7] C. Davis, R. Tanikella, T. Sung, P. Kohl, and G. May, "Optimization of variable frequency microwave curing using neural networks and genetic algorithms," in *Proc. 53rd Electron. Compon. Tech. Conf.*, New Orleans, LA, 2003, pp. 1718–1723.

[8] C. Davis, R. V. Tanikella, P. Kohl, and G. May, "Neural network modeling of variable frequency microwave curing," in *Proc. Electron. Compon. Technol. Conf.*, 2002, pp. 931–935.

[9] M. K. Ghosh and K. L. Mittal, *Polyimides: Fundamentals and Applications*. New York: Marcel Dekker, 1996.

[10] B. Geisler, B. Adams, and I. Ahmad, "Advanced process finds optoelectronic applications," *Adv. Packag.*, Apr. 2002.

[11] Y. J. Lee, B. T. Khuri-Yakub, and K. Saraswat, "Temperature measurement in rapid thermal processing using the acoustic temperature sensor," *IEEE Trans. Semiconductor Manufacturing*, vol. 9, no. 3, pp. 115–121, Aug. 1996.

[12] S. Morton, F. Degertekin, and B. T. Khuri-Yakub, "Ultrasonic sensor for photoresist process monitoring," *IEEE Trans. Semicond. Manuf.*, vol. 12, no. 3, pp. 332–339, Aug. 1999.

[13] J. Lu, K. Wakai, S. Takahashi, and S. Shimizu, "Acoustic computer tomographic pyrometry for two-dimensional measurement of gases taking into account the effect of refraction of sound wave paths," *Meas. Sci. Technol.*, vol. 11, pp. 692–697, Jun. 2000.

[14] R. H. Stones and P. J. Webb, "The application of acoustic pyrometry to gas temperature measurement and mapping," *IEE Colloquium on Ultrasound in the Process Ind.*, pp. 9/1–9/2, Sep. 1993.

[15] G. T. Herb and C. Fendrock, DuraMetrics, Inc., Sudbury, MA, "Ultrasonic thermometer system," U.S. patent 6,517,240, 2003.

[16] F. L. Degertekin, J. Pei, B. V. Honein, B. T. Khuri-Yakub, and K. C. Saraswat, "Thin film effects in ultrasonic wafer thermometry," in *Proc. IEEE Ultrasonics Symp.*, 1994, vol. 3, pp. 1337–1341.
[17] F. L. Degertekin, J. Pei, Y. J. Lee, B. T. Khuri-Yakub, and K. C. Saraswat, "*In-Situ* ultrasonic thermometry of semiconductor wafers," in *Proc. IEEE Ultrasonics Symp.*, 1993, vol. 1, pp. 375–377.
[18] J. Pei, F. L. Degertekin, B. V. Honein, B. T. Khuri-Yakub, and K. C. Saraswat, "In situ thin film thickness measurement using ultrasonics waves," in *Proc. IEEE Ultrasonics Symp.*, 1994, pp. 1237–1240.
[19] Y. J. Lee, C. H. Chou, B. T. Khuri-Yakub, and K. C. Saraswat, "Non-Invasive process temperature monitoring using laser-acoustic techniques," in *Proc. Symp. VLSI Technol.*, 1990, pp. 105–106.
[20] S. L. Morton, F. L. Degertekin, and B. T. Khuri-Yakub, "Ultrasonic cure monitoring of photoresist during pre-exposure bake process," in *Proc. IEEE Ultrasonics Symp.*, 1997, pp. 837–840.
[21] C. E. Wold, J. D. Sternhagen, R. D. Mileham, K. D. Mitzner, and D. W. Galipeau, "Temperature measurement using surface skimming bulk waves," in *Proc. IEEE Ultrasonics Symp.*, 1999, pp. 441–444.
[22] J. D. Sternhagen, C. E. Wold, W. A. Kempf, M. Karlgaard, K. D. Mitzner, R. D. Mileham, and D. W. Galipeau, "A novel integrated acoustic gas and temperature sensor," *IEEE Sens. J.*, vol. 2, no. 4, pp. 301–301, Aug. 2002.
[23] H. J. Mcskimin, "Measurement of elastic constants at low temperatures by means of ultrasonic waves—Data for silicon and germanium single crystals, and for fused silica," *J. Appl. Phys.*, vol. 24, pp. 988–997, Aug. 1953.
[24] T. M. Reeder and D. K. Winslow, "Characteristics of microwave acoustic transducers for volume wave excitation," *IEEE Trans. Microw. Theory Tech.*, vol. MTT-17, no. 11, pp. 927–941, Nov. 1969.
[25] B. T. Khuri-Yakub, G. S. Kino, and P. Galle, "Studies of the optimum conditions for growth of RF-sputtered ZnO films," *J. Appl. Phys.*, vol. 46, pp. 3266–3272, Aug. 1975.
[26] M. J. Vellekoop, A. Venema, C. C. G. Visser, and P. M. Sarro, "" Processing and passivation of zinc oxide films in silicon applications," *Amer. Ceramic Soc. Bull.*, vol. 69, pp. 1503–1505, 1990.
[27] F. S. Hickernell, "ZnO processing for bulk- and surface-wave devices," in *Proc. Ultrasonic Symp.*, 1980, pp. 785–794.
[28] Y. Kim, W. D. Hunt, F. S. Hickernell, R. J. Higgins, and C.-K. Jen, "ZnO films on $\{001\}$-Cut $\langle 100\rangle$-propagating GaAs substrates for surface acoustic wave device applications," *IEEE Trans. Ultrasonics, Ferroelectr. Freq. Control*, vol. 42, no. 3, pp. 351–361, May 1995.
[29] S. W. Wenzel and R. M. White, "Flexural plate-wave gravimetric chemical sensor," *Sens. Actuators A: Phys.*, vol. 22, pp. 700–703, 1990.
[30] S. L. Pinkett, "Techniques to facilitate the fabrication of ZnO-based thin film bulk acoustic wave devices," Ph.D.dissertation, Elect. Comput. Eng., Georgia Inst. of Technol., Atlanta, 2003.
[31] V. Ristic, *Principles of Acoustic Devices*. New York: Wiley, 1983.
[32] J. B. Lee, S. H. Kwak, and H. J. Kim, "Effects of surface roughness of substrates on the C-axis preferred orientation of ZnO films deposited by R.F. Magnetron sputtering," *Thin Solid Films*, vol. 423, pp. 262–266, 2003.
[33] B. T. Khuri-Yakub, J. G. Smits, and T. Barbee, "Reactive magnetron sputtering of ZnO," *J. Appl. Phys.*, vol. 52, pp. 4772–4774, Jul. 1981.
[34] N. J. Ianno, L. Mcconville, N. Shaikh, S. Pittaland, and P. G. Snyder, "Microstructural evolution and preferred orientation change of radio-frequency-magnetron sputtered ZnO thin films," *J. Vacuum Sci. Technol.: A*, vol. 14, pp. 1943–1948, May/Jun. 1996.
[35] J. C. Zesch, B. Hadimioglu, B. T. Khuri-Yakub, M. Lim, R. Lujan, and J. Ho, "Deposition of highly oriented low-stressed ZnO films," in *Proc. Ultrasonic Symp.*, 1991, pp. 445–447.
[36] A. Cimpoiasu, N. M. V. D. Pers, T. H. D. Keyser, A. Venema, and M. J. Vellekoop, "Stress control of piezoelectric ZnO films on silicon substrates," *Smart Mater. Structures*, vol. 5, pp. 744–750, 1996.
[37] Y. Chen, N. T. Tuan, Y. Segawa, H.-J. Ko, S.-K. Hong, and T. Yao, "Stimulated emission and optical gain in ZnO epilayers grown by plasma-assisted molecular-beam epitaxy with buffers," *Appl. Phys. Lett.*, vol. 78, pp. 1469–1471, 2001.
[38] H. Sheng, N. W. Emanetoglu, S. Muthukumar, B. V. Yakshinskiy, S. Feng, and Y. Lu, "Ta/Au Ohmic contacts to N-type ZnO," *J. Electron. Mater.*, vol. 32, pp. 935–938, 2003.
[39] B. J. Jin, S. Im, and S. Y. Lee, "Violet and UV luminescence emitted from ZnO thin films grown on sapphire by pulsed laser deposition," *Thin Solid Films*, vol. 366, pp. 107–110, 2000.
[40] T. Shibata, K. Unno, E. Makino, and S. Shimada, "Characterization of sputtered ZnO thin film as sensor and actuator for diamond AFM probe," *Sens. Actuators A: Phys.*, vol. 102, pp. 106–113, 2002.
[41] M. J. Vellekoop, C. C. G. Visser, P. M. Sarro, and A. Venema, "Compatibility of zinc oxide with silicon IC processing," *Sens. Actuators A: Phys.*, pp. 1027–1030, 1990.
[42] J. Rosenbaum, *Bulk Acoustic Wave Theory and Devices*. Norwood, MA: Artech House, 1988.
[43] X. Zhu, "Micromachined self-focusing acoustic wave transducers," M.S. thesis, Elect. Eng., Univ. Hawaii, Honlulu, 1997, pp. 79.
[44] R. Krimholtz, D. A. Leedom, and G. L. Matthaei, "New equivalent circuits for elementary piezoelectric transducers," *Electron. Lett.*, vol. 6, pp. 398–399, Jun. 1970.
[45] S. Sherrit, S. P. Leary, B. P. Dolgin, and Y. Bar-Cohen, "Comparison of the Mason and Klm equivalent circuits for piezoelectric resonators in the thickness mode," in *Proc. IEEE Ultrason. Symp.*, 1999, pp. 921–926.
[46] S. L. Morton, "Ultrasonic sensor for photoresist process monitoring," Ph.D. dissertation, Elect. Eng., Stanford Univ., Palo Alto, CA, 1999.
[47] "S-parameter techniques," Hewlett Packard Application Note 95–1.

Cleon E. Davis (M'06) received the B.S. and M.S. degrees in electrical engineering from Florida A&M University, Tallahassee, in 1995 and 2000, respectively, and the M.S. and Ph.D. degrees in electrical and computer engineering from the Georgia Institute of Technology, Atlanta, in 1999 and 2007, respectively.

He is currently a member of the Senior Technical Staff at The Johns Hopkins University Applied Physics Laboratory, Laurel, MD, where his research focuses on state estimation and sensor fusion. His other research interests are in the area of artificial intelligence applied to computer-integrated manufacturing of semiconductors and electronic packaging with an emphasis on modeling, optimization, diagnosis, and control of the fabrication equipment and processes.

Anthony Dickherber (S'00) received the B.S. and M.S. degrees in electrical engineering from the Georgia Institute of Technology (Georgia Tech), Atlanta, in 1999 and 2003, respectively. He is currently pursuing the Ph.D. degree in the School of Bioengineering at Georgia Tech.

While pursuing the M.S. degree, he spent four years at the Georgia Tech Research Institute in their Information Technology and Telecommunications Laboratory. He is also a Sam Nunn Security Program Fellow.

William D. Hunt (SM'04) is a Professor of Electrical Computer Engineering at the Georgia Institute of Technology (Georgia Tech), Atlanta, and is Adjunct Professor in the Department of Hematology and Oncology at the Emory University School of Medicine, Atlanta. He runs the Microelectronics Acoustics Group at Georgia Tech and has a diverse collection of graduate students which has included students from electrical engineering, biomedical engineering and chemistry. He joined the Electrical Engineering Faculty at Georgia Tech following completion of his Ph.D. degree. He holds eight U.S. patents and six provisional patents.

Dr. Hunt received the NSF Presidential Young Investigator Award in 1989, the DuPont Young Faculty Award in 1988, and the University of Alabama Distinguished Engineering Fellowship in 1994. He was a Rhodes Scholar Finalist in 1975. His "dog on a chip" invention which is a chip which can do specific molecular recognition of compounds in the vapor phase garnered worldwide press culminating in his appearance in the January 12, 2004 issue of *Time* magazine in their inaugural article on innovators. His area of expertise is in the area of microelectronic acoustic devices for wireless applications as well as chemical and biological sensors based on this technology. He has published over 70 papers in refereed journals and conference proceedings. He is a Senior Member of the IEEE and served as a Distinguished Lecturer for the IEEE Sensors Council from 2006 to 2008 and is currently serving as a Distinguished Lecturer for the IEEE Ultrasonics, Ferroelectrics, and Frequency Control Society.

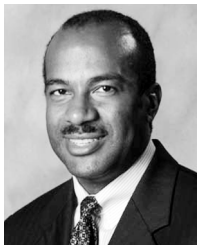

Gary S. May (M'90–SM'97–F'06) received the B.S. degree in electrical engineering from the Georgia Institute of Technology (Georgia Tech) in 1985 and the M.S. and Ph.D. degrees in electrical engineering and computer science from the University of California at Berkeley in 1987 and 1991, respectively.

He is currently a Professor and the Steve W. Chaddick School Chair of the School of Electrical and Computer Engineering at the Georgia Tech. In that capacity, he serves as the Chief Academic Officer of the school and provides leadership to over 110 faculty members and 2300 students in the sixth ranked electrical engineering and computer engineering programs in the nation. Prior to that, he served as the Executive Assistant to the President and Motorola Foundation Professor in the School of Electrical and Computer Engineering, Georgia Tech. His research is in the field of computer-aided manufacturing of integrated circuits, and his interests include semiconductor process and equipment modeling, process simulation and control, automated process and equipment diagnosis, and yield modeling.

Dr. May was Editor-in-Chief of IEEE TRANSACTIONS ON SEMICONDUCTOR MANUFACTURING from 1997–2001 and was a National Science Foundation "National Young Investigator" (1993–1998). He was a National Science Foundation and an AT&T Bell Laboratories Graduate Fellow, and has worked as a member of the technical staff at AT&T Bell Laboratories, Murray Hill, NJ. He is a member of the National Advisory Board of the National Society of Black Engineers (NSBE).